Petroleum Science 23 (2026) 2639–2654

Contents lists available at ScienceDirect

Petroleum Science

journal homepage: www.keaipublishing.com/en/journals/petroleum-science

Original Paper

Techno-economic co-optimization of CO_2 enhanced oil recovery strategies in a tight oil reservoir using coupled improved evolutionary algorithm and machine learning framework

Shu-Qin Wen [a], Bing Wei [a,*], Jun-Yu You [b,**], Nan-Jiang Leng [c], William Ampomah [d]

[a] State Key Laboratory of Oil and Gas Reservoir Geology and Exploitation, Southwest Petroleum University, Chengdu, 610500, Sichuan, China
[b] School of Petroleum and Natural Gas Engineering, Chongqing University of Science and Technology, Chongqing, 401331, China
[c] Daqing Oilfield Design Institute Co., Ltd., Daqing, 163000, Heilongjiang, China
[d] Petroleum Recovery Research Center, New Mexico Tech, Socorro, NM 87801, USA

ARTICLE INFO

Article history:
Received 10 October 2025
Received in revised form
21 January 2026
Accepted 21 January 2026
Available online 6 February 2026

Edited by Jia-Jia Fei

Keywords:
CO_2 enhanced oil recovery
Multi-objective optimization
Improved non-dominated sorting genetic algorithm II
Unconventional oil reservoir

ABSTRACT

Massive carbon dioxide (CO_2) emissions drive climate change. Injecting CO_2 into unconventional reservoirs achieves both enhanced oil recovery (EOR) and geological sequestration. However, simultaneously optimizing oil exchange ratio, CO_2 storage, and net present value remains challenging. This study develops an integrated machine learning (ML)-based framework for multi-objective optimization of CO_2-EOR. A high-resolution reservoir simulation was constructed from field data, and Latin hypercube sampling generated diverse scenarios for proxy training. Mantel's test quantified correlations between input parameters and performance metrics, showing that injection strategy strongly controls net present value, whereas geological properties dominate CO_2 storage. Three ML models—random forest (RF), support vector regression, and artificial neural networks—were evaluated, with RF selected for its superior performance on small datasets. RF was embedded into an improved non-dominated sorting genetic algorithm II, enhanced with grey difference degree, crowding distance, and adaptive differential evolution to improve diversity and efficiency. Finally, the technique for order preference by similarity to ideal solution ranked Pareto-optimal solutions through integrating oil productivity, storage, and economics. The proposed framework operationalizes simultaneous high-efficiency tight oil recovery and field-scale CO_2 geological storage, delivering quantitative design rules that embed low-carbon practice into upstream operations and advance the energy sector's greener and sustainable transition.

1. Introduction

In recent years, significant changes in the global climate system have been widely attributed to the increasing concentration of greenhouse gases, particularly the continuous accumulation of CO_2 in the atmosphere. CO_2 emissions not only contribute to global warming and the increased frequency of extreme weather events, but also exert profound impacts on the structure and functioning of ecosystems. Meanwhile, with the depletion of conventional hydrocarbon resources and the rising global energy demand, unconventional reservoirs have emerged as critical contributors to energy security (Chen et al., 2022). Unlike conventional reservoirs, unconventional formations typically exhibit highly complex pore structures, ultra-low permeability, and rapid energy depletion (Syed et al., 2022; Zuloaga et al., 2017). The injection of CO_2 into such reservoirs offers dual benefits: it enhances oil recovery (EOR) and facilitates long-term geological sequestration, aligning with carbon capture, utilization, and storage (CCUS) objectives (Farajzadeh et al., 2020; Zhao et al., 2025). However, the simultaneous optimization of CO_2 injection strategies to maximize oil recovery, storage capacity, and economic performance under complex geological constraints presents a significant technical challenge. The conflicting nature of these multiple objectives

* Corresponding author.
** Corresponding author.
E-mail addresses: bwei@swpu.edu.cn (B. Wei), youjunyu2013@gmail.com (J.-Y. You).
Peer review under the responsibility of China University of Petroleum (Beijing).

https://doi.org/10.1016/j.petsci.2026.01.040

further intensifies the complexity of operational design. Consequently, there is an urgent need for a robust multi-objective decision-making framework that can effectively mediate among trade-offs and guide the development of optimized strategies for unconventional reservoir exploitation.

Traditionally, optimization of CO_2-EOR projects in unconventional reservoirs relies on numerical simulation coupled with single-factor and multi-factor orthogonal experimental designs to assess CO_2 storage efficiency and hydrocarbon recovery (Chen et al., 2025b; Liu et al., 2021). These studies typically focus on the individual effects of operational parameters, while often overlooking the complex interdependencies and interactions among multiple variables, thereby increasing the risk of suboptimal decision-making. In recent years, due to the conflicting nature of objective functions and the presence of complex constraints in similar engineering scenarios, machine learning (ML) and multi-objective optimization algorithms have been widely applied to parameter optimization and injection strategy design in oil and gas development. Recent advancements have seen the integration of proxy modeling techniques to replace computationally expensive reservoir simulations, enabling more efficient and scalable exploration of optimal injection strategies under multi-variable conditions (Carpenter, 2022; Nguyen et al., 2024).

Wu et al. (2025) introduced a rapid optimization framework integrating multi-objective particle swarm (MOPSO), transformer, and long short-term memory network (LSTM) models to jointly optimize multi-level well scheduling and control consistency parameters, effectively maximizing both net present value (NPV) and CO_2 storage. Lu et al. (2025) incorporated numerical simulation with MOPSO and proposed a Pareto-based decision protocol to balance recovery and economic returns, particularly in optimizing surfactant injection strategies. Ding et al. (2024) utilized both single- and multi-objective PSO in combination with response surface methodology to enhance CO_2 huff-n-puff efficiency and sequestration performance in tight reservoirs. Their findings highlighted that each optimization mode and objective function necessitates tailored selection of dominant parameters. Amin and Mahdia (2014) pioneered the use of non-dominated sorting genetic algorithm II (NSGA-II) for the co-optimization of CO_2 storage and oil recovery. Building on this, Zhuang et al. (2024) developed a hybrid AI framework combining LSTM and NSGA-II for well placement and control parameter optimization in waterflooding, targeting maximum cumulative production and minimum water cut. Subsequently, the same research group proposed a Transformer-NSGA-III workflow to optimize both compositional and operational parameters in CO_2 mixed-gas huff-n-puff, aiming to simultaneously maximize CO_2 storage, recovery, and NPV (Zhuang et al., 2025). However, this work did not address demand-driven parameter selection, focusing solely on a predefined injection mode. These efforts demonstrate an increasing enthusiasm for ML-driven optimization in CO_2-EOR applications. However, most existing studies focus on the pairwise optimization of CO_2 storage, oil recovery, or NPV, while neglecting the integrated optimization of productivity, storage effectiveness, and profitability (Wen et al., 2025). Moreover, the expanding application of multi-objective optimization has exposed inherent inadequacies in traditional algorithms.

NSGA-II has demonstrated considerable effectiveness in multi-objective tasks such as CO_2-EOR parameter tuning and energy scheduling, owing to its elitism, non-dominated sorting, and crowding distance strategies (Dong et al., 2022; Wang et al., 2021). However, as problem dimensionality and sample complexity increase, several limitations have emerged in practical applications. For instance, crowding distance fails to capture true local diversit (Du et al., 2024), non-dominated sorting becomes computationally expensive with dense fronts (Kong et al., 2025), and static genetic parameters hinder adaptability in dynamic spaces (Zhao et al., 2019). To overcome these drawbacks, recent studies have proposed various enhancements. Shi and Xiong (2024) introduced a customized two-stage decoding strategy to accelerate convergence based on different optimization stages, along with adaptive and local search mechanisms to balance exploration and exploitation. Aghbari and Gujarathi (2023) introduced a hybrid of NSGA-II and bi-objective genetic programming to improve diversity. Chen et al. (2023) proposed p-NSGA-II, integrating preference-based selection to align with decision-maker interests while preserving robustness. These developments point to an active research trend aimed at improving convergence, diversity, and scalability. Clearly, improving the efficiency and solution quality of NSGA-II remains a key research priority in multi-objective optimization. This work contributes by refining NSGA-II to enhance its spatial exploration and ensure more uniform solution distribution, thereby better addressing the demands of complex engineering decision-making tasks.

Despite the availability of a well-structured and uniformly distributed Pareto front in multi-objective optimization, identifying a representative solution for practical deployment remains a key challenge. The inherent trade-off nature of Pareto sets precludes straightforward ranking, necessitating the application of robust multi-criteria decision-making techniques (Lin and Yeh, 2012). Among these, the technique for order preference by similarity to ideal solution (TOPSIS) stands out due to its conceptual clarity, computational efficiency, and numerical robustness (Han et al., 2025). Unlike analytic hierarchy process (AHP) or VIKOR, TOPSIS exhibits enhanced sensitivity to data fluctuations in high-dimensional objective spaces, making it particularly well-suited for rapid decision support in engineering optimization contexts (Das and Behera, 2024; Lin et al., 2021). When coupled with entropy-based weighting, this method mitigates subjective bias and improves the discriminative power of solution ranking. The integrated TOPSIS–entropy framework has demonstrated strong applicability in reservoir development, enabling a balanced evaluation of productivity, CO_2 storage potential, and economic viability (Chen et al., 2025a).

This study introduces an advanced ML-integrated workflow for the coordinated optimization of CO_2-EOR injection strategies in unconventional reservoirs, targeting the simultaneous maximization of oil exchange ratio (OER), CO_2 storage capacity, and NPV. A numerical model was first constructed using the geological, engineering, and field data from a depleted reservoir block. This model enabled the generation of a comprehensive database by simulating CO_2-EOR processes under various operational scenarios. Based on this database, a high-fidelity proxy model was developed, within which the improved NSGA-II (INSGA-II) algorithm was integrated to derive a smooth and accurate Pareto front. Subsequently, a comprehensive evaluation is performed using the TOPSIS method to rank the Pareto-optimal solutions, thereby facilitating efficient and precise decision-making in multi-objective optimization. The main contributions of this work are as follow: (1) A novel multi-objective optimization framework is proposed that yields a more comprehensive set of solutions while integrating both subjective and objective weighting factors. This framework simultaneously coordinates productivity, CO_2 storage, and economic performance, offering clear guidance for field-scale CO_2-EOR scheme selection. (2) The classical NSGA-II algorithm is improved by replacing the crowding distance with a composite metric that combines grey difference degree and crowding distance weighting. This effectively enhances the uniformity and distribution quality of the Pareto front. Moreover, a differential-based adaptive mechanism is implemented to dynamically adjust crossover and mutation probabilities, thereby reinforcing the algorithm's exploration capability and maintaining solution diversity. This integrated approach ensures not only the efficient and profitable use of CO_2 but also accounts for its sequestration

potential, offering a robust methodological foundation for intelligent decision-making in CO_2-EOR applications within unconventional reservoirs.

2. Reservoir description

The target block is the Ma18 fault block of the Triassic Baikouquan Formation (T_1b), located in the central part of Junggar Basin. Fig. 1 illustrates the numerical simulation model of the block. This study focuses exclusively on the T_1b_1 interval of the T_1b, which is further subdivided into three intervals according to lithology: $T_1b_1^1$, $T_1b_1^2$, and $T_1b_1^3$, from top to bottom. The porosity of this fault block ranges from a minimum of 6.7% to a maximum of 8.7%, with an average porosity of 7.4%. The permeability varies between 0.07 and 0.31 mD, with an average value of 0.19 mD. The surface crude oil density is 824 kg/m^3, and the gas-oil ratio is 156 m^3/m^3. A total of 44 vertical wells have been drilled in the study block, among which 14 wells have been shut in. The recovery factor relying solely on natural energy is only 10.38%, with relatively low single-well productivity. Subsequently, two wells were selected for acid fracturing followed by water injection to improve recovery. However, due to poor pore structure and strong interlayer heterogeneity, water flooding resulted in low sweep efficiency and unsatisfactory development performance. Given the poor performance of conventional water flooding, CO_2 injection is considered not only to enhance recovery but also to facilitate CO_2 sequestration. However, the effectiveness of CO_2-EOR is influenced by multiple factors, including reservoir properties and injection–production parameters. Therefore, optimizing operational parameters to balance injection and production efficiency is key to successful development.

3. Methodology

This study aims to establish an efficient and robust multi-objective optimization framework for CO_2-EOR in unconventional reservoirs, targeting the simultaneous maximization of OER, CO_2 storage capacity, and NPV. The framework integrates the INSGA-II algorithm with the TOPSIS decision-making method. A numerical reservoir model was first used to generate a foundational dataset for proxy model development. RF, SVR, and ANN models were trained, and the one with the best predictive performance was selected as the proxy model. A key innovation of this work is to propose an adaptive mechanism for dynamically adjusting crossover and mutation probabilities, coupled with a weighted scheme that integrates grey difference degree and crowding distance. This approach significantly improves the exploration capability of the population and preserves solution diversity, yielding a well-distributed and accurate Pareto front. As a result, decision-makers are provided with a richer set of viable options and are better equipped to analyze the trade-offs and evolving relationships among multiple objectives, thereby enabling more robust and precise strategy formulation.

3.1. Mantel's test

Mantel's test, originally proposed by Mantel (1967), evaluates the relationship between different variables by analyzing the correlation between distance matrices. It primarily consists of two components: correlation analysis and significance testing. In this study, the Pearson correlation analysis (Eq. (1)) is employed to quantify the degree of association among input variables. And a permutation test (Eq. (2)) is then used to assess the statistical significance, thereby exploring the influence of the output variable on the input variables.

$$r = \frac{\sum_{i<j}\left(x_{ij}-\bar{x}\right)\left(y_{ij}-\bar{y}\right)}{\sqrt{\sum_{i<j}\left(x_{ij}-\bar{x}\right)^2}\sqrt{\sum_{i<j}\left(y_{ij}-\bar{y}\right)^2}} \tag{1}$$

where $\bar{x}$ is the average of variable X, and $\bar{y}$ is the average of variable Y.

$$p = \frac{1+\sum_{i=1}^{N} I(|T_i| \geq |T_{\text{obs}}|)}{N+1} \tag{2}$$

$$T_{\text{obs}} = f(X, Y) \tag{3}$$

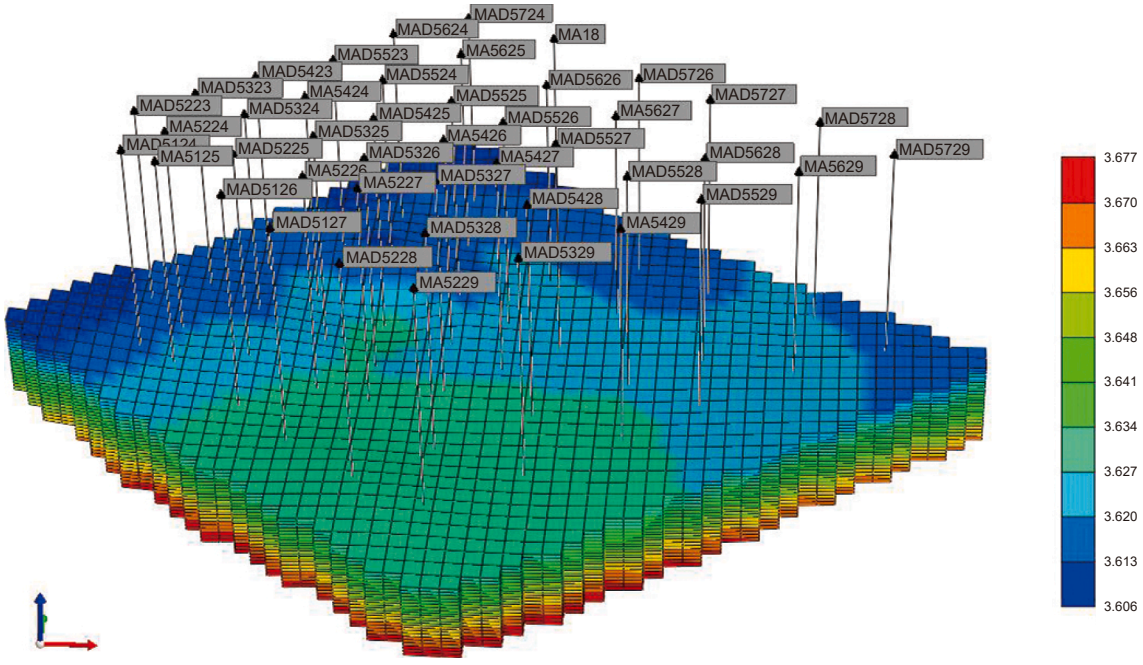

Fig. 1. The numerical simulation model of the target block in the study.

where T_i is the statistic obtained by the i-th permutation, T_{obs} is the average difference or Pearson correlation coefficient of variable X and Y, and N is the number of permutations.

3.2. Proxy model algorithm

Due to the limited size of the dataset, complex neural network models were not suitable for constructing the proxy model. Instead, RF, SVR, and ANN algorithms were employed to develop regression models, and the model with the best predictive performance was selected as the proxy model. To achieve optimal performance for each model, K-fold cross-validation coupled with GS was used to acquire the best hyperparameters (Kohavi, 1995). The overall ratio between the training data and the test data was 8:2. Considering the size of the dataset, the training data was further evenly divided into five subsets, as depicted in Fig. 2. In each iteration, four subsets were used for training and the remaining one for testing. The average error across the five iterations was taken as the final evaluation metric for the model. Compared to a train-test split, K-fold cross-validation reduces the bias caused by randomness, improves data utilization, and enhances the reliability of the prediction results.

RF is an ensemble learning model based on the bagging principle (Breiman, 1996). It constructs multiple decision trees and averages their predictions to achieve accurate final results. A decision tree is a top-down, tree-structured classifier that splits nodes into two child nodes based on specific splitting criteria and thresholds, continuing recursively until the input data are fully partitioned into distinct classes or regression intervals (Wen et al., 2023). Each tree is trained using bootstrap sampling to generate multiple training and test sets, where data are randomly selected with replacement. In each iteration, the data not included in the sample serve as out-of-bag data, which are used to evaluate the model's prediction performance. By randomly selecting subsets of input variables during the training process, RF promotes diversity among individual trees, enhances the model's generalization capability, and effectively prevents overfitting. As a result, RF has been widely applied to various classification and regression tasks.

SVR, proposed by Vapnik et al. (1996), is an extension of support vector machines (SVM) designed for nonlinear regression problems. The goal of SVR is to construct a regression function $f(x)$, similar to Eq. (4), by introducing an ε-insensitive loss function such that the prediction error for most training samples does not exceed a predefined margin. To handle nonlinear relationships, SVR employs kernel functions to map input data into a high-dimensional feature space. Commonly used kernels include the linear kernel, polynomial kernel, radial basis function (RBF) kernel, and sigmoid kernel. With the help of kernel methods, SVR can build accurate and efficient predictive models even with small datasets.

$$f(x) = \omega^{\mathrm{T}}\varphi(x) + b \tag{4}$$

where $f(x)$ is the regression function, $\varphi(x)$ is a kernel function, ω is the weight vector, and b is the bias vector.

ANN is a nonlinear model inspired by the information transmission and activation mechanisms of biological neurons. ANN is capable of modeling complex input–output relationships based on multilayer structures. The basic architecture of an ANN consists of three components: an input layer, one or more hidden layers, and an output layer (Kalil et al., 2024). These layers are fully connected to enable effective information transfer and feature extraction. ANN computes output values through forward propagation and updates weights via backpropagation of errors, allowing the model to adaptively learn high-order nonlinear relationships between inputs and outputs (David et al., 1986).

3.3. Multi-objective optimization process

3.3.1. NSGA-II

NSGA-II is an evolutionary algorithm for multi-objective optimization, proposed by Deb et al. (2002) as an enhancement of conventional GA. The core procedures of NSGA-II, including encoding, selection, crossover, and mutation, are similar to those of a GA. However, to ensure both convergence and diversity in multi-objective optimization, NSGA-II incorporates three key mechanisms: crowding distance, non-dominated sorting, and elitism strategy. The crowding distance, as defined in Eq. (5), represents the distance between a given individual and its neighboring individuals in the objective space. Fig. 3(a) illustrates how the crowding distance quantifies the distribution density of individuals on the Pareto front. In practical applications, individuals with larger crowding distances are preferred in order to maintain the diversity of the solution set.

$$CD_i = \sum_{m=1}^{M} \frac{f_m(i+1) - f_m(i-1)}{f_m^{\max} - f_m^{\min}} \tag{5}$$

Assume that there are n individuals on a given Pareto front, and each individual is associated with M objective values: $f_1(x), f_2(x), \ldots,$

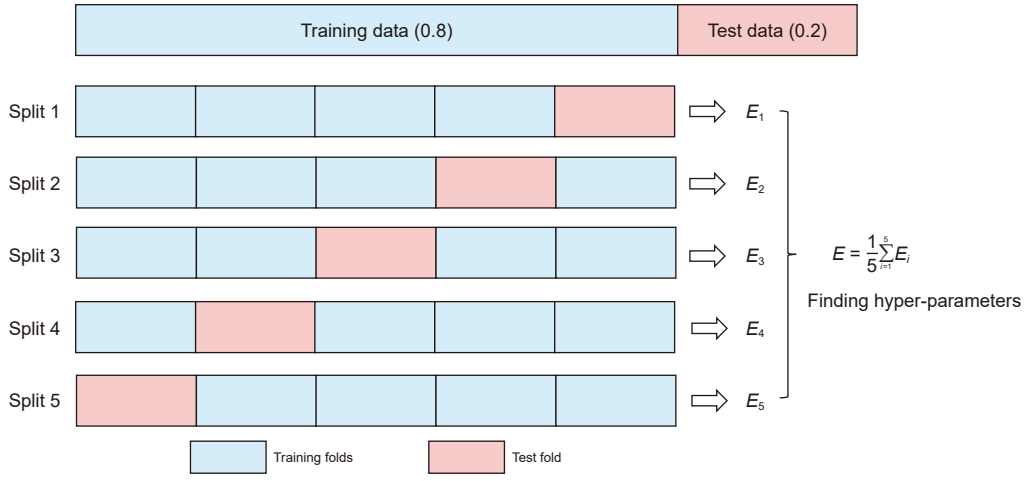

Fig. 2. K-fold partition diagram ($K = 5$).

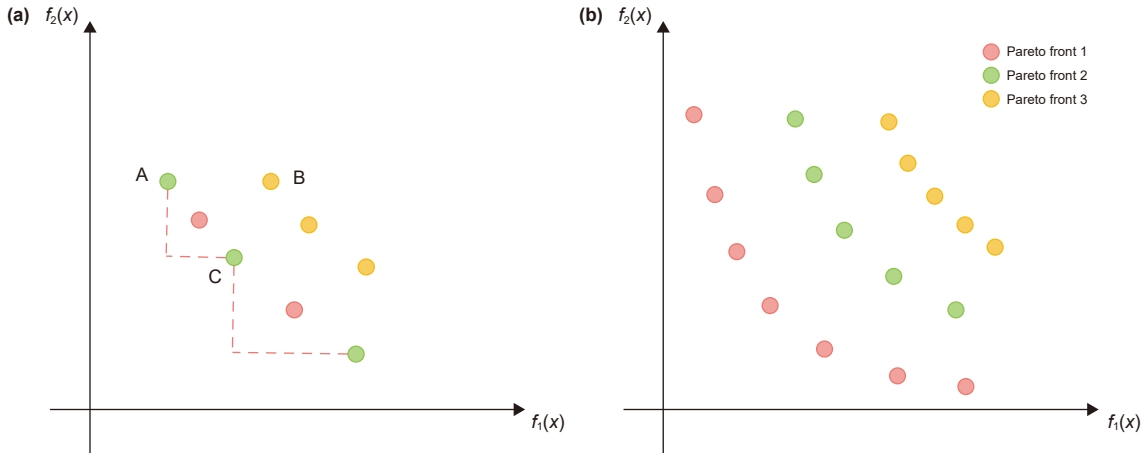

Fig. 3. (**a**) Schematic diagram of crowding distance, (**b**) illustration of Pareto front classification based on non-dominated sorting.

$f_M(x)$. In this study, $M = 3$. Where CD_i is the total crowding distance of individual i, $f_m(i+1)$ and $f_m(i-1)$ represent the objective function values of the two neighboring individuals adjacent to individual i in the m-th objective, $f_m^{\max}$ and $f_m^{\min}$ denote the maximum and minimum values of objective function f_m on the Pareto front, respectively.

The dominance relation is a criterion used in multi-objective optimization to compare the performance of two solutions. In the case of a bi-objective minimization problem, Fig. 3(a) exhibits that solution A dominates solution B because A performs better than B in objective $f_1(x)$. However, between A and C, A performs better in $f_1(x)$ while C performs better in $f_2(x)$, indicating a non-dominated relationship between them. Based on such comparisons, non-dominated sorting is employed to classify the population into multiple Pareto fronts, reflecting the quality ranking of individuals across all objectives. As shown in Fig. 3(b), individuals in front 1 are not dominated by any other solutions and thus represent the best front. The elitist strategy merges the parent and offspring populations, and selects the next generation based on non-dominated sorting and crowding distance. This approach helps preserve high-quality solutions and improves the algorithm's stability and convergence efficiency.

3.3.2. INSGA-II

Despite the robustness and wide applicability of NSGA-II in multi-objective optimization problems, it presents several inherent limitations in practical applications. For instance, the crowding distance is computed based on the normalized sum of local differences between neighboring solutions for each individual. However, this approach does not reflect the correlation among objective functions and fails to accurately capture the true sparsity of the solution set in high-dimensional objective space, which may result in uneven solution distributions (Zheng and Doerr, 2023). In addition, different problems exhibit varying sensitivities to parameter settings. If the crossover and mutation probabilities are not properly determined, the search direction and convergence speed of the population may be adversely affected (Feng et al., 2024).

To overcome the limitations discussed above, an improved NSGA-II (INSGA- II) algorithm is proposed in this study. First, a weighted combination of grey difference degree and crowding distance is introduced (Eq. (6)) to improve solution diversity. The grey difference degree, defined as the complement of the grey relational grade (Eq. (7)), evaluates the dissimilarity between candidate solutions and a reference sequence. The grey difference degree is computed to reduce the likelihood of preserving similar individuals in the population. Meanwhile, the crowding distance ensures that widely spread individuals are preserved to enhance coverage of the Pareto front. In addition, an adaptive strategy based on differential information is applied to regulate the crossover and mutation rates. Specifically, for individuals with large fitness differences or high population diversity, the crossover probability is increased to enhance exploration. For well-adapted or converging individuals, the mutation probability is raised to avoid premature convergence. The pseudocode of INSGA-II is presented in Table 1.

$$F = \lambda CD_i + (1-\lambda)(1-\gamma_i) \tag{6}$$

$$\gamma_i = \frac{1}{n}\sum_{k=1}^{n}\frac{\Delta_{\min} + \rho\Delta_{\max}}{\Delta_i(k) + \rho\Delta_{\max}} \tag{7}$$

where F is the solution sorting metric, λ is the weighting coefficient, which is set to 0.5 in this study. γ_i denotes the grey relational grade, $\Delta_i(k)$ represents the absolute difference between the reference sequence and the comparative sequence at time point k, $\Delta_{\min}$ and $\Delta_{\max}$ are the global minimum and maximum differences, respectively. And ρ is the distinguishing coefficient, $\rho \in (0,1)$.

To verify the performance improvement of the INSGA-II over the classical NSGA-II, benchmark testing was conducted using the DTLZ test (Manuel et al., 2023). Considering the improvement characteristics of INSGA-II, two representative functions prone to local optima, namely DTLZ1 and DTLZ5 (seeing the details of these two functions in Appendix), were selected for testing. In order to intuitively evaluate the convergence and diversity of the algorithm, the inverted generational distance (IGD) (Eq. (8)) was employed (Sun et al., 2019). IGD measures the average distance from each point on the Pareto front to its nearest solution in the obtained set, thus reflecting both the proximity and coverage of the solution set relative to the true Pareto front. A smaller IGD value implies superior convergence behavior and broader coverage of the true Pareto front. IGD is widely used as a comprehensive indicator of multi-objective optimization algorithm performance.

$$\mathrm{IGD} = \frac{1}{|P|}\sum_{i=1}^{|P|}\min_{i=1}^{|A|}\sqrt{\sum_{m=1}^{M}\left(\frac{f_m(p_i) - f_m\left(a_j\right)}{f_m^{\max} - f_m^{\min}}\right)^2} \tag{8}$$

Table 1
The pseudocode of INSGA-II.

Algorithm: INSGA-II	
Input: m, n	
1:	$P = \Phi$, $i = 1$
2:	P=Randominitiate (P)/*Initialize population*/
3:	While $\neg\tau$ do/*Termination condition check*/
4:	Q = MatingSlection (P);/*Mating selection*/
5:	Q = AdapitiveVariation (Q);/*Adaptive cross-mutation*/
6:	R=PUQ;/*Combine parent and offspring populations*/
7:	Compute function value (R);/*Compute the function value of each individual*/
8:	(F_1,F_2, …,F_l) = nondominatedsort (R)/*Stratify all individuals*/
9:	While $\|P\|+F_j \leq n$ do/*Compute the GRD of each individual*/
	Compute grey relation degree (F_i);
	$P = P + F_j$ and $i = i+1$;
	Compute grey dissimilarity score (D_i);
10:	End while
11:	While $\|P\|+F_j \leq n$ do/*Compute the crowding distance of each individual*/
	Compute crowding distance (CD_i);
	$P = P + CD_j$ and $i = i+1$;
12:	End while
13:	Compute combined distance (C_i);/*Fuse crowding and dissimilarity scores*/
14:	The last front to be include: $F_l = C_i$;
15:	If $\|P\| = n$ then
	Return P;
16:	Else Compute combined distance (C_l);/*Compute the combined distance of the last layer*/
	The number of points to be chosen from F_l: $k = n-\|P\|$;/*Determine the number of individuals in the last front*/
	Choose k members one at a time from F_l to construct P;
17:	End if
18:	End while

where P denotes a set of uniformly distributed solutions on the true Pareto front, $f_m^{\max}$ and $f_m^{\min}$ represent the maximum and minimum values of the m-th objective in P, respectively. $p_i \in P, i = 1,2,3,\ldots,|P|$, $a_j \in A, j = 1,2,3,\ldots,|A|$, $m = 1,2,3,\ldots,M$, and M is the number of objectives.

Fig. 4 illustrates the multi-objective optimization results for the DTLZ1 and DTLZ5 test functions using NSGA-II and INSGA-II, respectively. As displayed in Fig. 4(a) and (c), the solutions obtained using the traditional NSGA-II tend to cluster in specific regions, leading to an uneven distribution. This phenomenon indicates that when dealing with complex multi-objective problems, NSGA-II may lack the ability to explore the entire search space uniformly, thereby compromising the comprehensiveness and diversity of the optimization results. In contrast, the solutions generated by INSGA-II are more uniformly and continuously distributed across the Pareto front, as showed in Fig. 4(b) and (d), demonstrating a more complete and balanced set of alternatives.

IGD serves as a direct and quantitative measure of the convergence process. To enable a consistent performance comparison, the maximum number of iterations for each test function was set to 600. As illustrated in Fig. 5, while both NSGA and INSGA exhibit a declining trend in IGD values over successive iterations, INSGA achieves a more rapid reduction and stabilizes earlier. This indicates that the proposed improvements contribute significantly to enhancing the convergence rate and maintaining solution diversity throughout the optimization process.

3.4. TOPSIS

TOPSIS is a classical multi-attribute decision-making method (Hwang et al., 1993). Its core idea is to evaluate each alternative based on its relative closeness to the positive ideal solution (PIS) and negative ideal solution (NIS). The PIS represents the optimal combination of attribute values, while the NIS corresponds to the worst-case combination. The TOPSIS procedure consists of several steps: normalization of the decision matrix, construction of the weighted normalized matrix, determination of the PIS and NIS, calculation of the Euclidean distances from each alternative to the ideal and anti-ideal solutions, and finally, evaluation of the relative closeness to the ideal solution (Huang et al., 2023).

Assuming there are m alternatives and n evaluation criteria, the initial decision matrix is constructed as shown in Eq. (9), followed by vector normalization (Eq. (10)). After assigning a weight w_j to each criterion, the weighted normalized matrix $\mathbf{v}_{ij} = w_j \cdot r_{ij}$ is derived. The PIS and NIS are then identified (Eq. (11)), and the distances to these ideal points are calculated using Euclidean metrics (Eq. (12)). The relative closeness values are computed accordingly (Eq. (13)) to enable ranking of the alternatives.

$$\mathbf{X} = \begin{bmatrix} x_{11} & x_{12} & \cdots & x_{1n} \\ x_{21} & x_{22} & \cdots & x_{2n} \\ \vdots & \vdots & \ddots & \vdots \\ x_{m1} & x_{m2} & \cdots & x_{mn} \end{bmatrix} \tag{9}$$

$$r_{ij} = \frac{x_{ij}}{\sqrt{\sum_{i=1}^{m} x_{ij}^2}} \tag{10}$$

$$\begin{cases} V^+ = \left\{v_1^+, v_2^+, \ldots, v_n^+\right\} = \left\{v_j^+ = \max_i \left\{\mathbf{v}_{ij}\right\} | i = 1,2,\ldots,m\right\} \\ V^- = \left\{v_1^-, v_2^-, \ldots, v_n^-\right\} = \left\{v_j^- = \min_i \left\{\mathbf{v}_{ij}\right\} | i = 1,2,\ldots,m\right\} \end{cases} \tag{11}$$

$$\begin{cases} S_i^+ = \sqrt{\sum_{j=1}^{n} \left(\mathbf{v}_{ij} - v_j^+\right)^2} \\ S_i^- = \sqrt{\sum_{j=1}^{n} \left(\mathbf{v}_{ij} - v_j^-\right)^2} \end{cases} \tag{12}$$

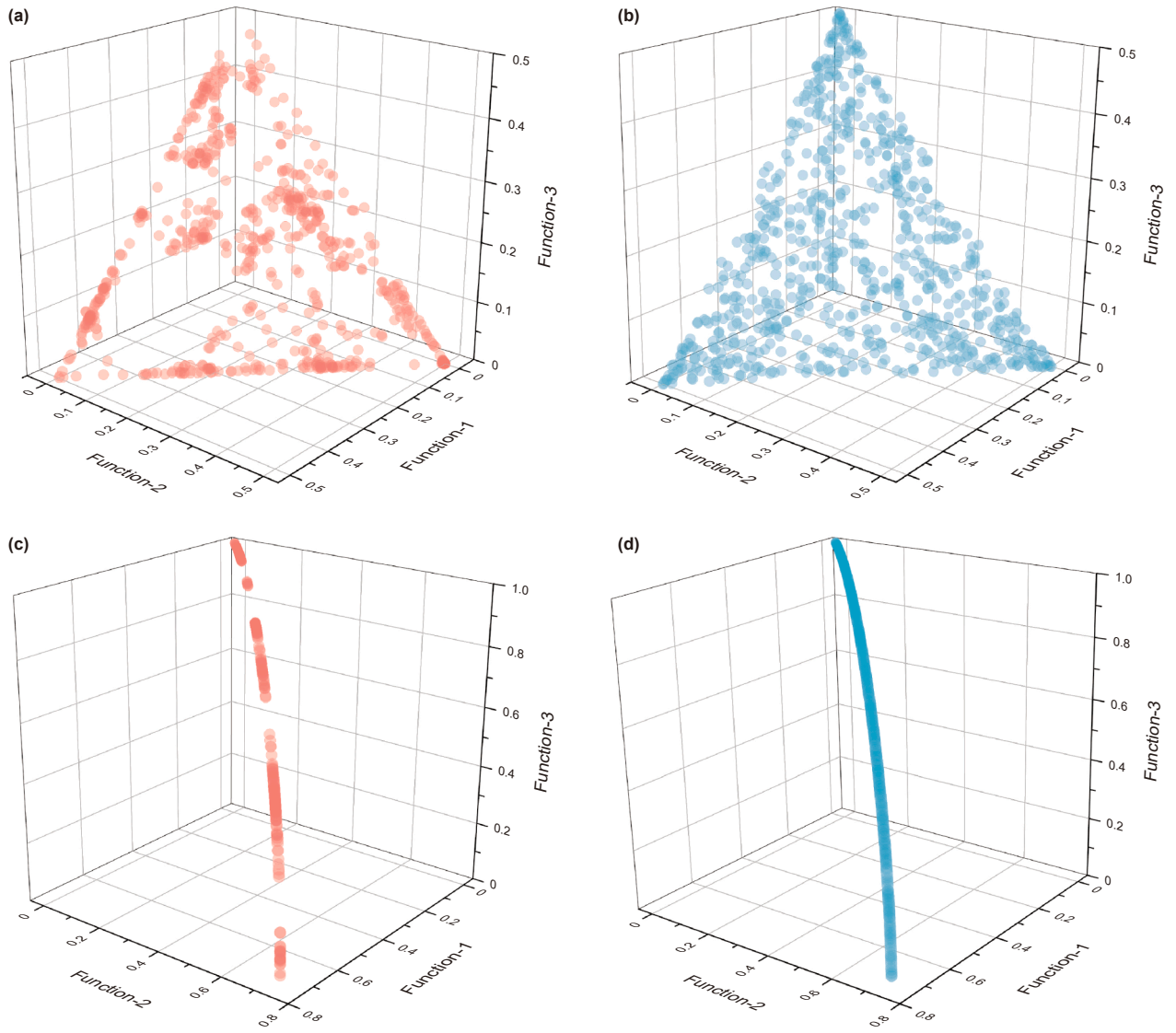

Fig. 4. Optimization results for DTLZ test functions: (**a**) DTLZ1 results using NSGA-II, (**b**) DTLZ1 results using INSGA-II, (**c**) DTLZ5 results using NSGA-II, and (**d**) DTLZ5 results using INSGA-II.

$$C_i = \frac{S_i^-}{S_i^+ + S_i^-} \tag{13}$$

where **X** is the initial decision matrix, r_{ij} denotes the normalized attribute values, V^+ and V^- represent the PIS and NIS, respectively. S_i^+ is the distance from a given alternative to the PIS, S_i^- is the distance to the NIS, and C_i denotes the relative closeness to the ideal solution.

In the framework of the TOPSIS model, criterion weights exert a critical influence on the reliability of the final ranking. If weights are improperly assigned, the evaluation results may become skewed or misleading. Conventional weighting techniques include equal weighting and subjective assignment. To incorporate both expert preferences and intrinsic data characteristics, this study adopts a combined subjective–objective weighting approach. Specifically, the final weight vector w_j is constructed by proportionally integrating the entropy-based objective weights (w_{je}) and the subjective weights (w_{js}), as defined in Eq. (16). The entropy weight method, grounded in information theory (Eq. (14)), quantifies the degree of dispersion for each attribute. Criteria with higher variability yield lower entropy values, resulting in greater weights. This hybrid scheme enhances the robustness and explanatory power of the evaluation process by harmonizing empirical data-driven insights with expert judgment.

$$e_j = -k\sum_{i=1}^{m} r_{ij}\ln r_{ij}, k = \frac{1}{\ln m} \tag{14}$$

$$w_{\mathrm{je}} = \frac{1-e_j}{\sum_{j=1}^{1}\left(1-e_j\right)} \tag{15}$$

$$w_j = \gamma w_{\mathrm{je}} + (1-\gamma)w_{\mathrm{js}} \tag{16}$$

where e_j denotes the information entropy, k is the normalization constant, w_{je} represents the weight derived from the entropy method, w_{js} is the subjective weight, w_j is the final integrated weight, and γ is the weighting coefficient used for combining the two weight vectors, $\gamma = 0.5$ in this study.

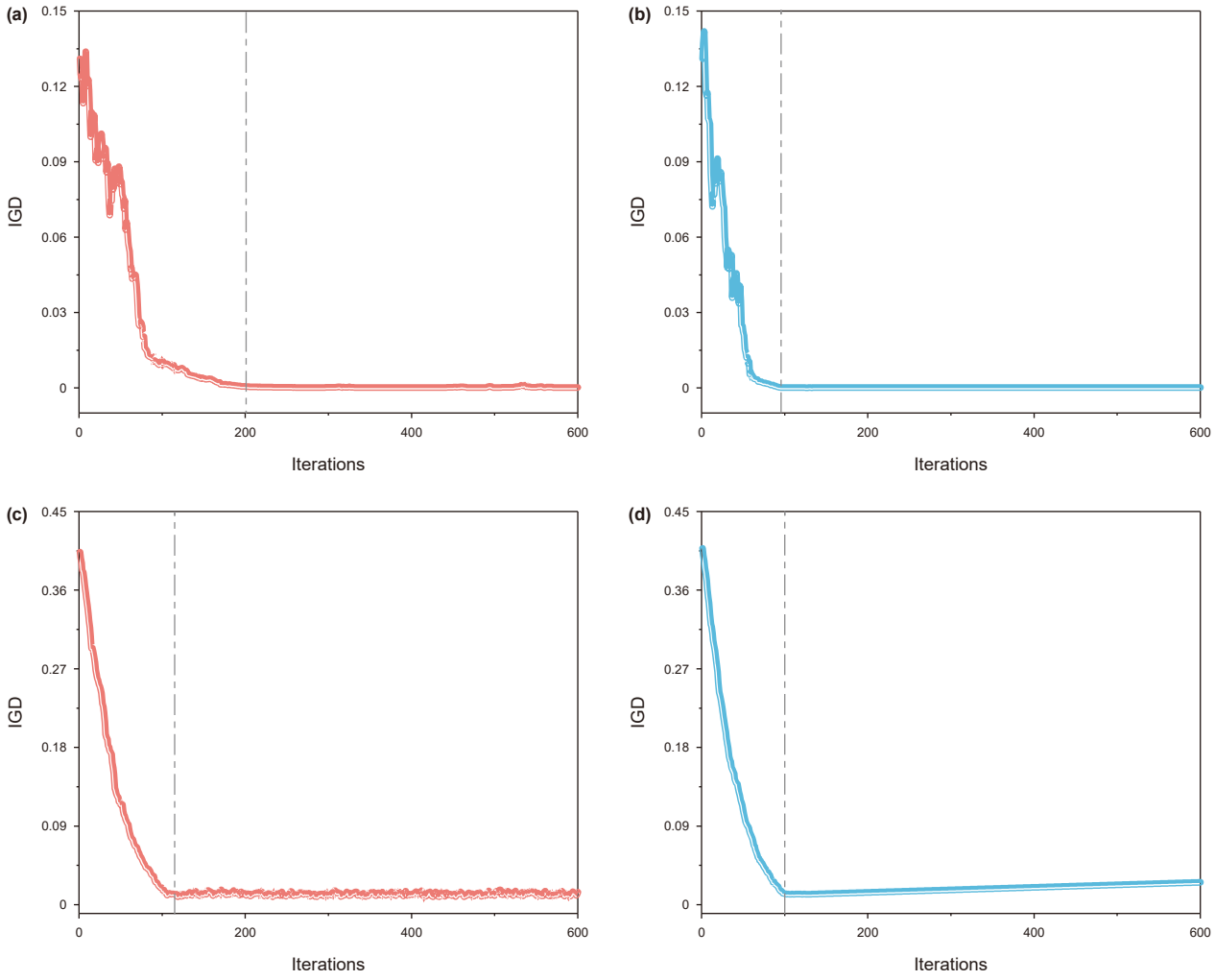

Fig. 5. Comparison of IGD performance on DTLZ test functions: (**a**) DTLZ1 optimized by NSGA-II, (**b**) DTLZ1 optimized by INSGA-II, (**c**) DTLZ5 optimized by NSGA-II, and (**d**) DTLZ5 optimized by INSGA-II. The dashed line indicates the iteration number at which the IGD value stabilizes.

4. The proposed framework

The proposed framework consists of five main steps: data acquisition and preprocessing, correlation analysis, proxy model construction, multi-objective optimization, and comprehensive assessment. The workflow of the proposed methodology is presented in Fig. 6.

Step 1. Data acquisition and preprocessing. The numerical simulation model was constructed based on the field development data of the Ma18 fault block under depletion conditions. LHS was employed to generate 200 experimental designs based on the operational parameters summarized in Table 2. These designs comprise both continuous CO_2 injection and WAG injection modes. Subsequently, the 200 generated scenarios were compiled to form the foundational dataset for constructing the proxy model.

Step 2. Correlation analysis. Prior to proxy model development, the Mantel's test was employed to assess the correlation between input and output variables. This approach computes the interrelationships among input features using Pearson correlation coefficients and determines the statistical significance of input–output dependencies through permutation-based significance testing. By uncovering the global response structure among variables, this method facilitates the elimination of redundant features, supports informed variable selection, and enhances the robustness and explanatory capacity of the proxy model.

Step 3. Proxy model construction. RF, SVR, and ANN were respectively used to construct multi-input, multi-output prediction models. To mitigate the impact of stochastic fluctuations and reduce the risk of overfitting, *K*-fold cross-validation in combination with GS was employed for hyperparameter optimization. The proxy model used the operational parameters as input variables, including CO_2 injection mode, gas injection rate (GIR), water injection rate (WIR), gas injection time (GIT), water injection time (WIT), injection-production ratio (IPR), and oil production rate (OPR). The corresponding output responses were OER, CO_2 storage capacity, and NPV.

Step 4. Multi-objective optimization. The INSGA-II algorithm was employed to explore the optimal Pareto front, with the objective of simultaneously maximizing the three target functions. The INSGA-II algorithm replaces the traditional crowding distance with a composite metric that integrates grey difference degree and crowding distance, while adaptively adjusting the crossover and mutation probabilities based on the differential method. These improvements are designed to enhance the algorithm's global search capability and ensure the quality and uniformity of the Pareto front distribution.

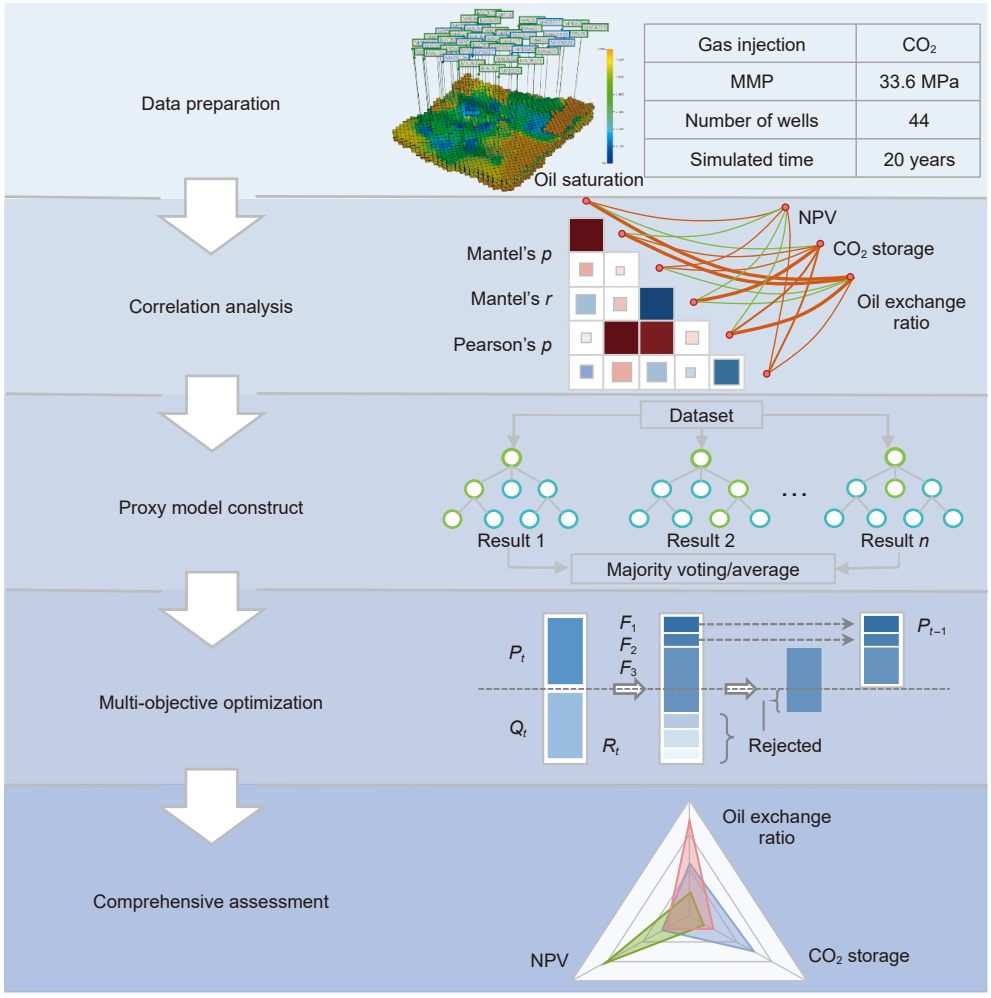

Fig. 6. The workflow of the proposed work.

Table 2
The variation ranges of operational parameters.

Features	Injection mode	GIR, t/d	ROP	IPR	GIT, m	WIT, m
Value range		30–70	GIR × IPR	0.7–1.4	12	0
	COI				8	4
	WAG				6	6
					4	8

Step 5. Comprehensive assessment. A comprehensive assessment of the Pareto-optimal solutions was conducted using the TOPSIS method, with an integrated weighting scheme derived from the combination of entropy-based objective weights and expert-assigned subjective weights. The entropy weighting approach utilizes information entropy to quantify the variability and informational contribution of each criterion, ensuring that indicators with greater discrimination receive higher weights. The inclusion of subjective weights enables the incorporation of domain-specific preferences during decision-making. This hybrid weighting strategy enhances the credibility, interpretability, and robustness of the multi-criteria evaluation process.

5. Case study

5.1. Data acquisition and preprocessing

The study focuses on the Ma18 fault block of the T_1b, targeting the T_1b_1 subunit within the T_1b member. A reservoir simulation model was developed using available field data, comprising 23 stratified layers in total: layers 1 to 7 correspond to $T_1b_1^1$, layers 8 to 15 to $T_1b_1^2$, and layers 16 to 23 to $T_1b_1^3$. A total of 44 vertical wells have been drilled in the block, with 14 wells shut in following depletion due to insufficient economic performance. Based on the current well pattern, a reverse nine-spot configuration was proposed for CO_2-EOR, with injection modes including continuous injection (COI) and WAG. The final well configuration consists of 8 injection wells and 36 production wells.

A total of 200 injection scenarios were generated using LHS within the operational parameter ranges specified in Table 2. These scenarios were implemented in the numerical model with a simulation period of 20 years. To enable direct comparison of different CO_2 injection strategies, one injection cycle was standardized to one year. For WAG, the combined duration of CO_2 and water injection within a cycle was constrained to one year. In contrast, under COI, CO_2 was injected for the full year, with no water injection involved.

This study aims to simultaneously maximize three key objectives: OER, CO_2 storage capacity, and NPV. The economic analysis accounts for several factors, including but not limited to CO_2 pricing, water costs, capital expenditure (CAPEX), and the inflation rate. NPV, as the principal economic evaluation metric, is calculated according to Eq. (19) (Morgan et al., 2023; Wang et al., 2021), with variable definitions and values provided in Table 3. Given that the CO_2-EOR operation is conducted using the existing well infrastructure, CAPEX is excluded from the economic assessment.

Table 3
Summary of economic parameters.

Terms	Definition	Value used
r_o	Oil price	65 $/bbl
r_w	Cost of water injection	1.03 $/stb
$r_{w,pro}$	Water treatment/recycling	0.64 $/stb
r_{CO_2}	Cost of CO_2 injection	0.85 $/MSCF
$r_{CO_2,p}$	Cost of purchased CO_2	1.72 $/MSCF
$r_{CO_2,pro}$	CO_2 treatment/recycling	2 $/MSCF
q_o	Oil production at n-th year	/
$q_{w,inj}$	Injected water at n-th year	/
$q_{w,pro}$	Produced water at n-th year	/
$q_{CO_2,inj}$	Injected CO_2 at n-th year	/
$q_{CO_2,pro}$	Produced CO_2 at n-th year	/
n	Year index	/
r	Rate of inflation	5%
CAPEX	Capital expenditure	0

$$\mathrm{NPV} = \sum_{n=1}^{T} \frac{C_n(x)}{(1+r)^n} - \mathrm{CAPEX} \tag{19}$$

$$C_n(x) = q_o r_o - q_{w,inj} r_w - q_{w,pro} r_{w,pro} - q_{CO_2,inj} r_{CO_2} - q_{CO_2,inj} r_{CO_2,p} - q_{CO_2,pro} r_{CO_2,pro} \tag{20}$$

This study considered two injection modes: COI and WAG. To facilitate their inclusion in the proxy model training, categorical encoding was performed using the one-hot encoding (Rodriguez et al., 2018). This technique maps categorical variables into binary vectors, where each vector has a value of 1 at the position corresponding to the category and 0 elsewhere, thereby preserving the categorical nature without introducing ordinal bias. Accordingly, COI was encoded as (1, 0), and WAG as (0, 1). The feature parameters after preprocessing is presented in Fig. 7. Before building the proxy model, Z-score standardization was applied to all variables to remove the effects of differing.

5.2. Mantel's test analysis

To quantitatively explore the structural influence of CO_2 injection operational parameters on OER, CO_2 storage capacity, and NPV, the Mantel's test was applied to evaluate the pairwise associations between variable matrices. Fig. 8 illustrates the outcomes of the Mantel's test in two components. The lower-left triangle shows a heatmap of Pearson correlation coefficients among the operational parameters. The color gradient indicates correlation strength and direction, with blue indicating positive correlation and red negative. Darker shades (or larger heatmap blocks) correspond to stronger correlations.

The upper-right triangle visualizes the correlations between each operational variable and the three optimization objectives. The color of the connecting lines indicates the level of statistical significance: orange lines represent statistically significant correlations ($P < 0.01$), while green lines represent non-significant associations ($P \geq 0.05$). Line thickness corresponds to the magnitude of the Pearson correlation coefficient, with thicker lines indicating stronger relationships. This visual encoding of both statistical significance and correlation strength facilitates intuitive interpretation of how operational parameters impact optimization performance.

The analysis demonstrates that NPV exhibits the highest sensitivity to changes in CO_2 injection operational parameters. Significant positive correlations were observed between NPV and variables such as injection mode, effective water injection volume (WIV), WIT and GIT, indicating that injection-related costs serve as the primary economic drivers. Conversely, the relationship between CO_2 injection parameters and CO_2 storage capacity was found to be weak yet statistically significant, suggesting that operational design exerts only a secondary influence on CO_2 storage performance. This observation aligns with prior research (Dai et al., 2014; Yue et al., 2022), which emphasizes that although operational optimization can enhance CO_2-EOR outcomes, fundamental reservoir characteristics—such as porosity, permeability, and depth—remain the dominant factors controlling CO_2 storage capacity. Overall, the results of the Mantel's test confirm the statistical relevance of operational parameters in explaining variability across all three optimization objectives. Furthermore, the integrity and consistency of the dataset support its suitability for use in proxy model construction.

5.3. Proxy model performance evaluation

The predictive performance of the RF, SVR, and ANN models was evaluated, and the model demonstrating the highest predictive accuracy was selected as the proxy model. A combination of 5-fold cross-validation and GS was applied to systematically determine the optimal hyperparameters for each model. The candidate hyperparameter ranges are presented in Table 4. For the RF model, the key hyperparameters included the number of trees (to balance prediction accuracy and model stability), tree depth (to mitigate overfitting or underfitting), and the random seed (to control stochastic effects and ensure reproducibility). In the SVR model, the regularization parameter (C) is a positive constant that governs the trade-off between model complexity and training error. For the ANN model, hyperparameter tuning focused on the number of hidden layers ($N_{\text{hidden layers}}$), the number of neurons per layer (N_{neurons}), and the activation function. The final optimal hyperparameter settings are shown in Table 5. During 5-fold cross-validation, each dataset was partitioned into training and test subsets at a 4:1 ratio.

Fig. 9 illustrates the cross-validation performance of the RF, SVR, and ANN models under their respective optimal hyperparameter configurations. In each plot, the proximity of the data points to the reference line with a slope of 1 signifies the degree of agreement between predicted and simulated values. The shaded regions represent the 95% confidence intervals, indicating the range within which the true mean value is expected to fall with 95% probability. These intervals serve as a measure of the model's reliability in estimating the mean response; a narrower interval generally corresponds to higher predictive confidence. Among the three models, the RF model (Fig. 9(a–c)) demonstrates the best overall performance, as evidenced by the close alignment of its confidence interval with the reference line. In contrast, regardless of the model used, predictions of CO_2 storage capacity show the weakest performance. This result aligns with the findings of the Mantel test, which indicated the lowest correlation and consistency between CO_2 storage and the input operational parameters.

To quantitatively assess model performance across the three optimization objectives, Fig. 10 illustrates the average relative errors for the RF, SVR, and ANN models. The RF model achieved training errors of 0.44% for OER, 2.86% for CO_2 storage capacity, and 0.28% for NPV. The corresponding test errors were 0.69%, 5.21%, and 0.36%, respectively. As detailed in Table 6, the RF model consistently outperforms the SVR and ANN models across all targets. This superior predictive capability is likely due to the "bootstrap sampling" strategy, which randomly samples both training instances and features. Such an approach mitigates overreliance on individual data points, thereby enhancing generalizability and robustness, particularly when dealing with limited

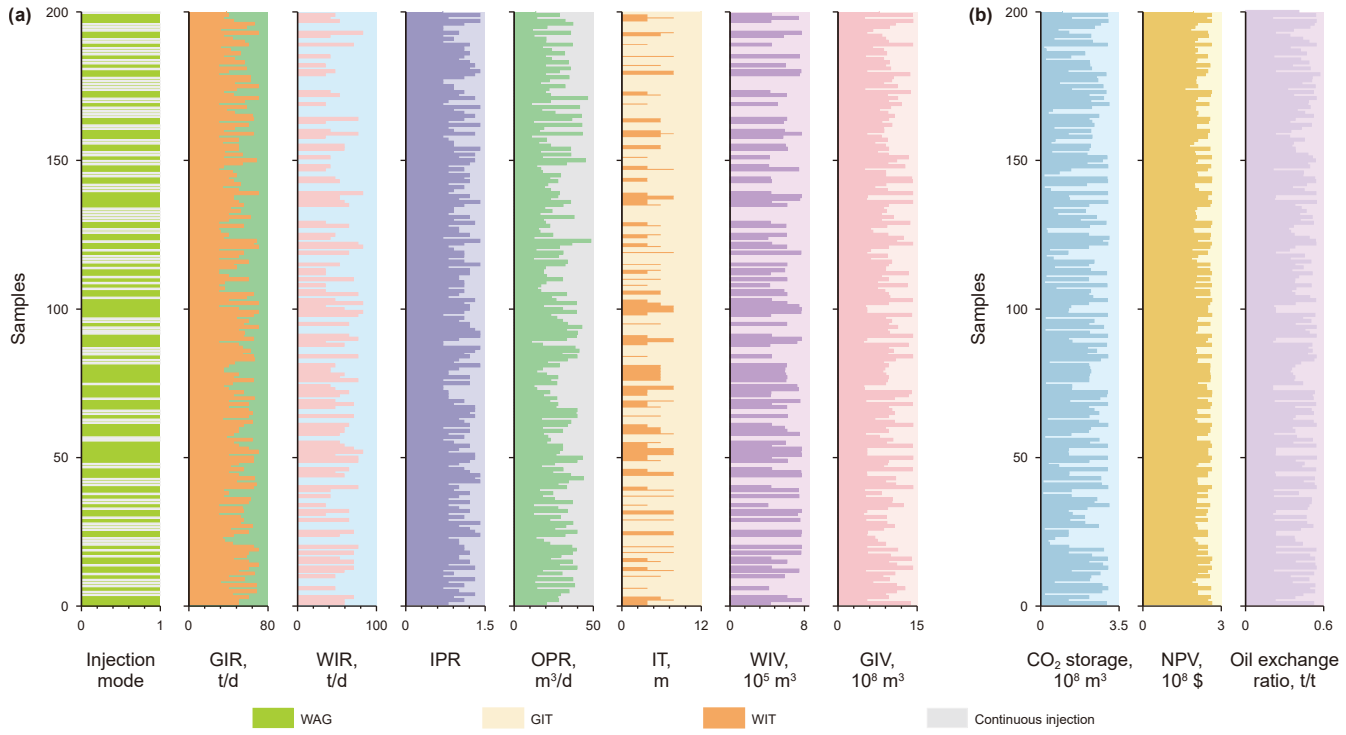

Fig. 7. Plots of the characteristic variables: (**a**) the operational parameters, (**b**) three optimization objectives.

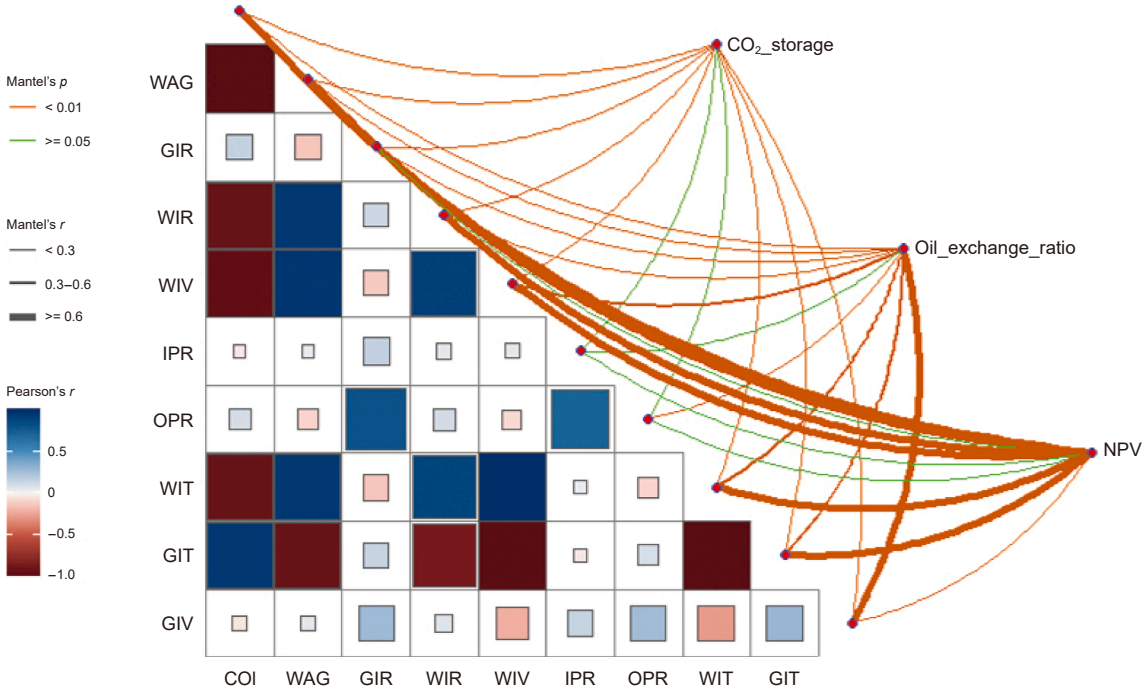

Fig. 8. The results analysis of Mantel's test.

datasets. Based on these findings, the RF model was adopted as the proxy model for subsequent optimization tasks.

5.4. Multi-objective optimization analysis

The proxy model was integrated into the INSGA-II framework to identify optimal injection strategies within the operational bounds defined in Table 2. For each candidate solution, the proxy model predicted the corresponding OER, CO_2 storage capacity, and NPV. These outputs were subjected to non-dominated sorting to construct the optimal Pareto front, which was subsequently compared to that generated by the standard NSGA-II algorithm. Fig. 11 illustrates the result of the optimal Pareto front, where circles highlight non-dominated solutions discovered by INSGA-II

Table 4
The range of hyperparameters of RF, SVR, and ANN model.

Model	RF	SVR	ANN
Hyperparameters range	The number of trees: {50, 100, 200, 300}, the maximum depth: {10,11, …,30}, random state: {1,2, …100}	Kernel function: sigmoid, polynomial, RBF, *C*: {0.1, 0.5, 1, 2, 3, 4}	$N_{\text{hidden layers}}$: {1,2,3}, N_{neurons}: {10,20,..,80}, activation function: sigmoid, ReLU, tanh

Table 5
The optimal hyperparameters of RF, SVR, ANN model.

Model	RF	SVR	ANN
The optimal hyperparameters	The number of trees: 200, the maximum depth: 24, random state: 45	Kernel function: Sigmoid, C: 3	$N_{\text{hidden layers}}$: 2, $N_{\text{neurons 1}}$: 40, $N_{\text{neurons 2}}$: 50, activation function: ReLU

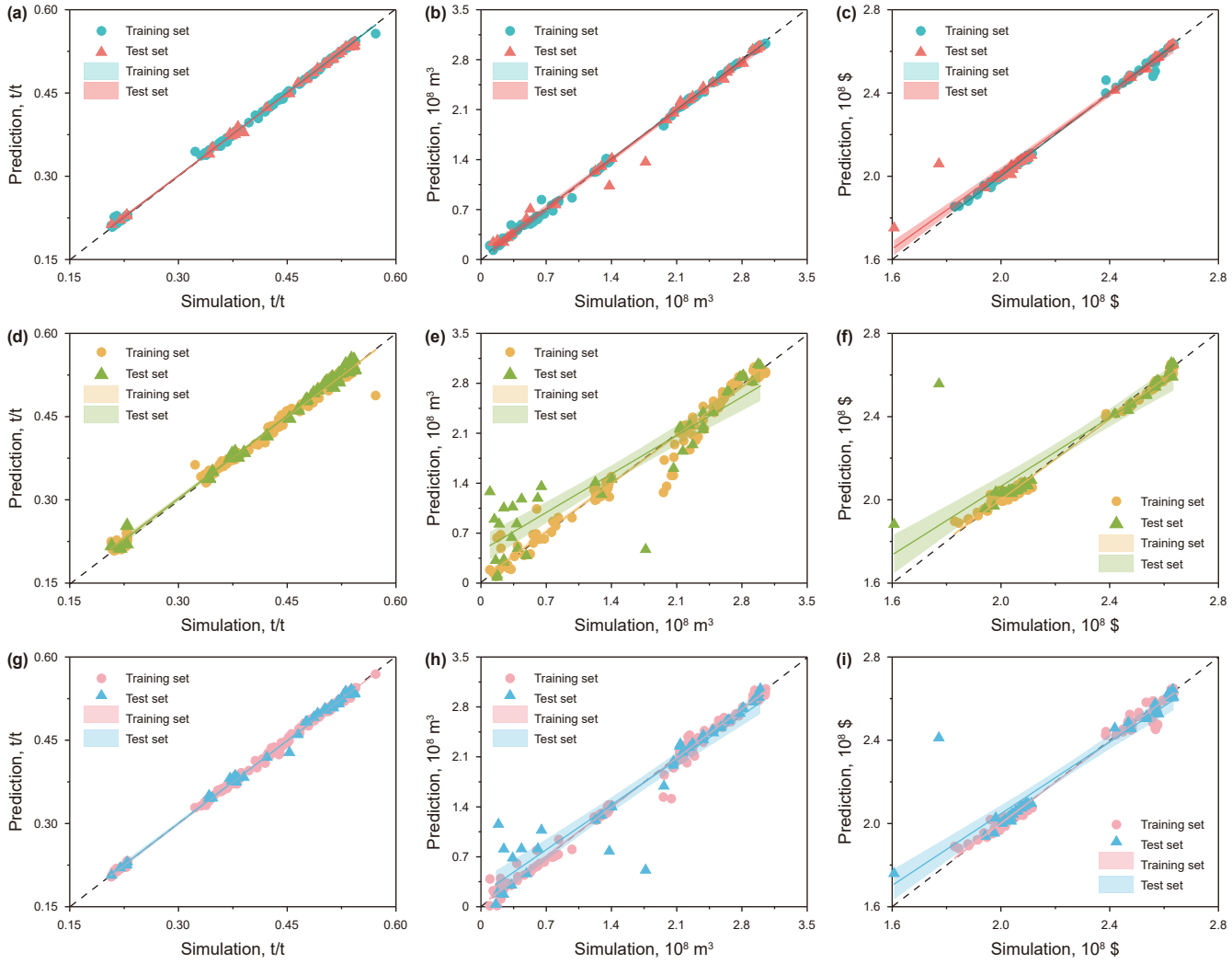

Fig. 9. The cross-plot analysis of RF model, SVR model and ANN model: (**a**) OER of RF model, (**b**) CO_2 storage capacity of RF model, (**c**) NPV of RF model, (**d**) OER of SVR model, (**e**) CO_2 storage capacity of SVR model, (**f**) NPV of SVR model, (**g**) OER of ANN model, (**h**) CO_2 storage capacity of ANN model, and (**i**) NPV of ANN model. The dashed line represents a slope of 1, while the solid line indicates the linear regression of the predicted versus simulated values. A solid line slope closer to 1 indicates higher prediction fidelity.

but missed by the conventional NSGA-II. These solutions demonstrate superior performance, particularly in terms of NPV and OER, thereby significantly improving the overall diversity of the solution set. Moreover, the solutions obtained by INSGA-II are more evenly distributed, effectively eliminating the clustering effect observed in the standard NSGA-II outcomes. Although the INSGA-II algorithm introduces significant improvements over NSGA-II, the runtime of NSGA-II was 4 min 50 s, while that of INSGA-II

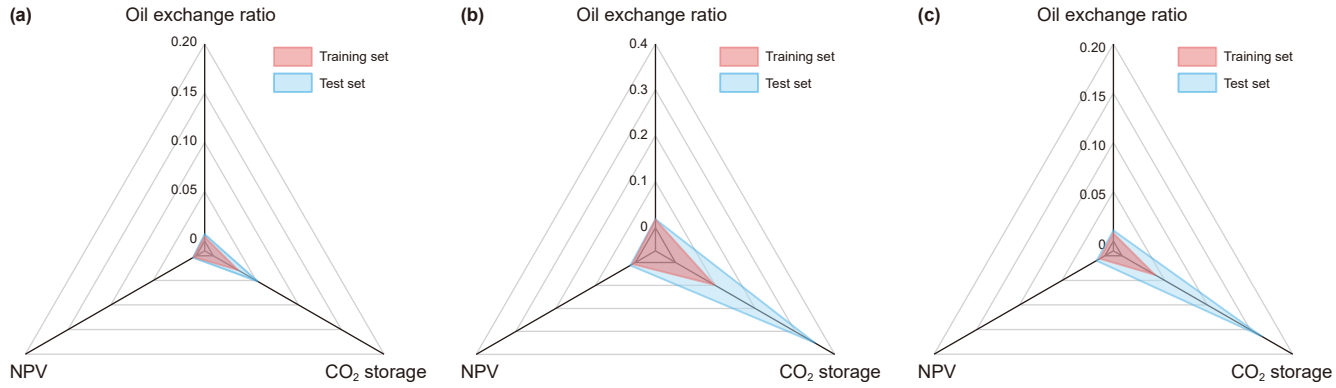

Fig. 10. The relative error of different models: (**a**) the relative error of RF model, (**b**) the relative error of SVR model, and (**c**) the relative error of ANN model.

Table 6
The relative error of different models.

Model	Data type	OER	CO_2 storage	NPV
RF	Training	0.44%	2.86%	0.28%
	Test	0.69%	5.21%	0.36%
SVR	Training	1.80%	34.95%	0.8%
	Test	1.85%	9.72%	1.31%
ANN	Training	0.78%	3.87%	0.61%
	Test	1.07%	16.35%	0.98%

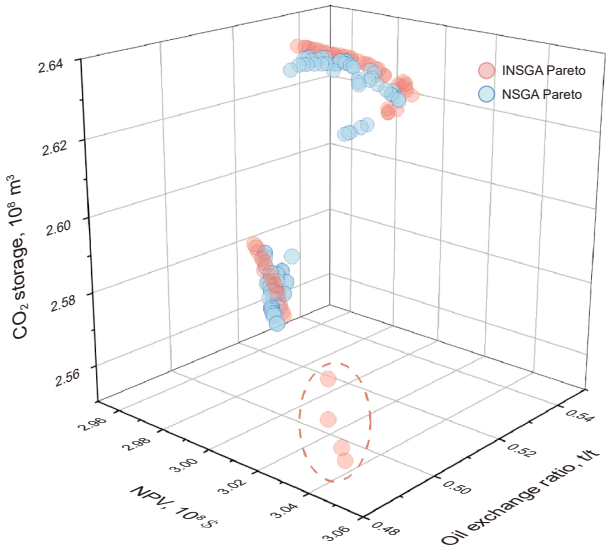

Fig. 11. Three-dimensional Pareto fronts generated by NSGA-II and INSGA-II.

was 5 min 20 s, with a difference of only 30 s. The computations were performed on a system equipped with Windows 10, an Intel(R) Core(TM) i3-6100 CPU, and an NVIDIA GeForce GT 1030 GPU. These results indicate that the proposed method has a substantially lower computational cost compared with traditional numerical simulation methods, demonstrating its strong potential for broad practical application.

To facilitate a visual assessment of solution distributions, Fig. 12 presents multi-angle projections of the Pareto fronts derived from both NSGA-II and INSGA-II. Compared to the NSGA-II, INSGA-II yields a more uniform spread of solutions and uncovers additional high-quality non-dominated solutions, particularly in the NPV dimension. Moreover, the improved algorithm effectively filters out suboptimal dominated solutions, reducing the risk of convergence to local optima. Across both benchmark test functions (Fig. 4) and field-scale optimization problems, INSGA-II consistently enhances the exploration of the objective space. The resulting Pareto fronts exhibit superior uniformity and continuity, leading to more comprehensive and diverse solution sets.

5.5. Comprehensive assessment analysis

Traditional multi-objective optimization techniques often employ a weighted-sum strategy to convert multiple objectives into a single scalar objective. While straightforward, this method rigidly adheres to predefined preferences, potentially excluding alternative solutions aligned with other trade-offs. Furthermore, it yields only a singular outcome, thus obscuring the structural diversity and interpretability of potential options. To address these limitations, this study retains the full set of non-dominated solutions along the Pareto front and applies a structurally informed ranking using the TOPSIS method with composite weighting. This allows for more nuanced exploration of objective trade-offs and aligns with diverse decision-making preferences.

The entropy-derived weights quantitatively capture the variability of each indicator based on the degree of information entropy. Fig. 12 illustrates the box plots of the three optimization objectives, revealing their inherent discriminability characteristics. A larger IQR indicates a higher degree of data dispersion, which corresponds to a higher assigned weight. The calculated IQR values are 0.0293 for NPV, 0.0455 for OER, and 0.0412 for CO_2 storage. Results show that the OER exhibits the highest entropy-based weight, followed by CO_2 storage, while NPV has the lowest. This weighting mechanism prioritizes indicators with high variability and strong discriminative power, thereby enhancing the objectivity and sensitivity of the overall evaluation. Furthermore, the final composite weight w_j is obtained by integrating entropy-based weights w_{je} with decision-maker-defined subjective weights w_{js}, thus offering a synergistic weighting strategy that reflects both data-driven insights and expert judgment. This dual-weighting approach increases the robustness, adaptability, and explanatory value of the multi-criteria decision-making process.

Table 7 summarizes the operational parameters of the selected schemes under various scenarios, along with the assigned subjective preference profiles. In Case 1, the multi-objective optimization problem is reduced to a single-objective formulation via equal-ratio weighting, followed by the selection of the solution maximizing that objective. In contrast, Cases 2, 3, and 4 leverage the TOPSIS method to prioritize NPV, OER, and CO_2 storage capacity, respectively. Under these scenarios, the subjective weight for the target objective is increased to 1.3, while the other two

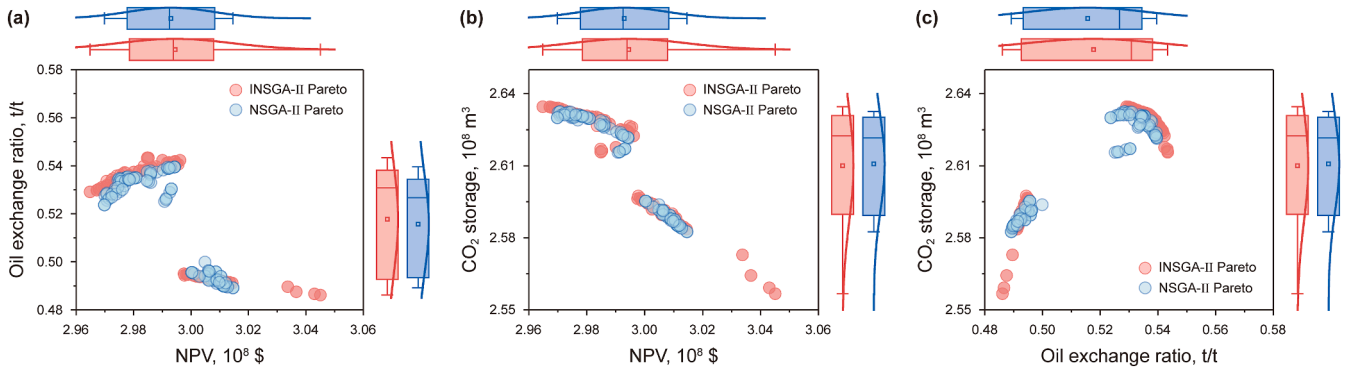

Fig. 12. Multi-perspective projections of the Pareto front solutions: (**a**) projection viewed from the CO_2 storage capacity axis, (**b**) projection viewed from the OER axis, (**c**) projection viewed from the NPV axis. The box plots visualize the interquartile range (IQR: 75%–25%), providing insight into the spread and variability of the solution distributions from each objective's perspective.

Table 7
Results of scheme selection and subjective weight assignment.

Case number	Injection mode	GIR, t/d	IPR	GIT, m	WIT, m	NPV, 10^8 $	OER, t/t	CO_2 storage, 10^8 m^3
Case 1	WAG	46.7	1.3	8	4	Geometric weighting		
Case 2	WAG	30.4	0.8	8	4	1.3	1.0	1.0
Case 3	WAG	67.8	1.4	8	4	1.0	1.3	1.0
Case 4	WAG	69.2	0.9	8	4	1.0	1.0	1.3

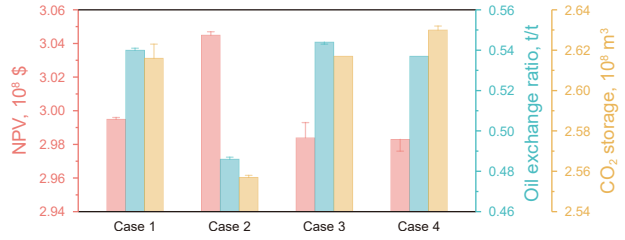

Fig. 13. Comparison of the three objective indicators across different decision scenarios.

remain at 1.0. Fig. 13 presents the performance of the three indicators across various scenarios, where bar heights denote proxy model predictions and error bars reflect CMG simulation results. It can be observed that the predicted results closely match the simulated ones, indicating that the proposed optimization framework exhibits a certain degree of robustness and applicability. As summarized in Table 8, although the numerical differences among competing solutions are relatively minor, the TOPSIS-based ranking demonstrates substantial decision-making value, particularly in resolving close-call trade-offs.

By incorporating engineering constraints and stakeholder preferences, the method facilitates the recommendation of context-appropriate optimal schemes. Given that the Pareto-optimal solutions obtained from INSGA-II inherently reflect well-balanced trade-offs, the overall solution set exhibits a degree of "equifinality". From a decision science perspective, the ranked outcomes underline the robustness and interchangeability of the top-performing solutions. Even with minor perturbations in specific criteria, the performance gaps between the optimal and near-optimal alternatives remain marginal, thereby enhancing the adaptability and resilience of implementation strategies. This highlights the practical utility of the proposed framework in supporting robust and flexible engineering decisions.

Table 8
Comparison of the three objective indicators under different scenarios.

Case number	NPV, 10^8 $	CO_2 storage, 10^8 m^3	Oil exchange ratio, t/t	C_i of TOPSIS
Case1	2.995	2.626	0.540	/
Case2	3.045	2.557	0.486	0.81
Case3	2.984	2.617	0.544	0.96
Case4	2.983	2.630	0.537	0.86

6. Conclusions

This study proposes an integrated and innovative framework to tackle the inherent complexity of dynamic modeling and multi-objective optimization in CO_2-EOR operations. By coupling high-fidelity numerical simulations with advanced ML algorithms, the framework elucidates the underlying interactions between injection parameters and performance metrics. An accurate and robust multi-objective proxy model was developed using synthetic datasets derived from field-calibrated simulations. Subsequently, the hybrid INSGA-II and TOPSIS approach enabled rapid and efficient optimization of CO_2-EOR strategies, simultaneously maximizing oil recovery, CO_2 storage, and economic returns. The framework effectively integrates data-driven modeling with expert-informed decision support, offering actionable insights. Key conclusions are summarized as follows.

(1) Mantel's correlation analysis indicates that among the three performance indicators, CO_2 operational parameters exert the most significant influence on NPV, while their correlation with CO_2 storage is weak. This corroborates prior findings that geological parameters such as porosity and permeability are the dominant factors affecting CO_2 storage.
(2) The RF model outperformed both SVR and ANN in predictive accuracy and robustness, and was thus selected as the proxy model. Its high fidelity facilitates rapid evaluation of operational strategies under various injection scenarios, predicting OER, CO_2 storage, and NPV with minimal error.

(3) The integration of the proxy model with the INSGA-II algorithm allowed for efficient surrogate-assisted multi-objective optimization. The INSGA-II framework introduces a novel combination of grey difference degree and crowding distance, coupled with a differential evolution-inspired adaptive mechanism for tuning crossover and mutation rates. This significantly improves search diversity and solution quality across the Pareto front.

(4) To facilitate practical decision-making, TOPSIS was employed with a hybrid weighting strategy incorporating both entropy-based objective weights and expert-defined subjective preferences. This dual-weighting mechanism enables the identification of optimal trade-off solutions that balance maximum NPV with acceptable oil recovery and CO_2 storage performance, thereby providing a technically and economically viable roadmap for CO_2-EOR in unconventional reservoirs.

Declaration of competing interest

The authors declare that they have no known competing financial interests or personal relationships that could have appeared to influence the work reported in this paper.

Acknowledgements

The authors gratefully acknowledge financial support from the National Key Research and Development Program of China (2023YFE0120700), National Science and Technology Major Project of China (2025ZD1408303), National Natural Science Foundation of China (52304023), Natural Science Foundation of Chongqing (CSTB2022NSCQMSX0403).

Appendix

The DTLZ test functions are widely used to evaluate and compare the performance of multi-objective evolutionary algorithms. They can simulate various Pareto front structures and assess the algorithms' convergence, diversity, and robustness. The DTLZ1 and DTLZ5 functions are defined by Eqs. (A.1) and (A.2), respectively.

$$\text{DTLZ1}\quad \begin{cases} \text{Min } f_1(x) = \frac{1}{2}x_1x_2(1+g(x)) \\ \text{Min } f_2(x) = \frac{1}{2}x_1(1-x_2)(1+g(x)) \\ \text{Min } f_3(x) = \frac{1}{2}(1-x_1)(1+g(x)) \\ g(x) = 100\left[k + \sum_{i=3}^{7}\left((x_i-0.5)^2 - \cos(20\pi(x_i-0.5))\right)\right] \end{cases} \tag{A.1}$$

$$\text{DTLZ5}\quad \begin{cases} \text{Min } f_1(x) = (1+g(x))\cos(\theta_1\pi/2)\cos(\theta_2\pi/2) \\ \text{Min } f_2(x) = (1+g(x))\cos(\theta_1\pi/2)\sin(\theta_2\pi/2) \\ \text{Min } f_3(x) = (1+g(x))\sin(\theta_1\pi/2) \\ \theta_i = \frac{\pi}{4(1+g(x))}(1+2g(x)x_i) \\ g(x) = \sum_{i=3}^{7}(x_i-0.5)^2 \end{cases} \tag{A.2}$$

where k denotes the number of redundant variables that define the complexity of $g(x)$, while x_1 and x_2 are the decision variables that control the shape of the Pareto front.

References

Al-Aghbari, M., Gujarathi, A.M., 2023. Hybrid approach of using bi-objective genetic programming in well control optimization of waterflood management. Geoenergy Sci. Eng. 228, 211967. https://doi.org/10.1016/j.geoen.2023.211967.

Amin, S.M., Mahdia, M.S., 2014. Co-optimization of carbon dioxide storage and enhanced oil recovery in oil reservoirs using a multi-objective genetic algorithm (NSGA-II). Pet. Sci. 11, 460–468. https://doi.org/10.1007/s12182-014-0362-1.

Breiman, L., 1996. Bagging predictors. Mach. Learn. 24, 123–140. https://doi.org/10.1023/A:1018054314350.

Carpenter, C., 2022. Machine learning optimizes production in an unconventional reservoir. J. Petrol. Technol. 74, 77–79. https://doi.org/10.2118/0722-0077-JPT.

Chen, H., Liu, X., Zhang, C., et al., 2022. Effects of miscible degree and pore scale on seepage characteristics of unconventional reservoirs fluids due to supercritical CO_2 injection. Energy 239, 122287. https://doi.org/10.1016/j.energy.2021.122287.

Chen, X., Li, K., Zhang, L., et al., 2023. Robust optimization of energy-saving train trajectories under passenger load uncertainty based on p-NSGA-II. IEEE T. Transp. Electr. 9, 1826–1844. https://doi.org/10.1109/TTE.2022.3194698.

Chen, Y., He, G., Fang, Y., et al., 2025a. Carbon emission evaluation system for foundation construction based on entropy–TOPSIS and *K*-means methods. Sustainability 17, 369. https://doi.org/10.3390/su17010369.

Chen, Z., Zhao, X., Zhu, H., et al., 2025b. Engineering factor analysis and intelligent prediction of CO_2 storage parameters in shale gas reservoirs based on deep learning. Appl. Energy 377, 124642. https://doi.org/10.1016/j.apenergy.2024.124642.

Dai, Z., Middleton, R., Viswanathan, H., et al., 2014. An integrated framework for optimizing CO_2 sequestration and enhanced oil recovery. Environ. Sci. Technol. Lett. 1, 49–54. https://doi.org/10.1021/ez4001033.

David, E.R., Geoffrey, E.H., Ronald, J.W., 1986. Learning representations by back-propagation errors. Nature 323, 533–536. https://doi.org/10.1038/323533a0.

Das, U., Behera, B., 2024. Geospatial assessment of ecological vulnerability of fragile Eastern duars forest integrating GIS-Based AHP, CRITIC and AHP-TOPSIS models. Geomat. Nat. Hazards Risk 15, 2330529. https://doi.org/10.1080/19475705.2024.2330529.

Deb, K., Pratap, A., Agarwal, S., et al., 2002. A fast and elitist multiobjective genetic algorithm: NSGA-II. IEEE Trans. Evol. Comput. 6, 182–197. https://doi.org/10.1109/4235.996017.

Ding, S., Liu, Q., Li, P., et al., 2024. An efficient hybrid methodology for optimization of CO_2 Huff-n-Puff EOR and sequestration in tight oil reservoirs. Int. J. Greenh. Gas Control 132, 104062. https://doi.org/10.1016/j.ijggc.2024.104062.

Dong, W., Huang, Y., Lehane, B.M., et al., 2022. Multi-objective design optimization for graphite-based nanomaterials reinforced cementitious composites: a data-driven method with machine learning and NSGA-II. Constr. Build. Mater. 331, 127198. https://doi.org/10.1016/j.conbuildmat.2022.127198.

Du, J., Liu, R., Cheng, D., et al., 2024. Enhancing NSGA-II algorithm through hybrid strategy for optimizing maize water and fertilizer irrigation simulation. Symmetry 16, 1062. https://doi.org/10.3390/sym16081062.

Farajzadeh, R., Eftekhari, A.A., Dafnomilis, G., et al., 2020. On the sustainability of CO_2 storage through CO_2-Enhanced oil recovery. Appl. Energy 261, 114467. https://doi.org/10.1016/j.apenergy.2019.114467.

Feng, T., Li, J., Jiang, H., et al., 2024. The optimal global path planning of mobile robot based on improved hybrid adaptive genetic algorithm in different tasks and complex road environments. IEEE Access 12, 18400–18415. https://doi.org/10.1109/ACCESS.2024.3357990.

Han, Z., Han, W., Song, X., et al., 2025. A new multi-objective optimization model for an integrated energy system based on life-cycle composite technical, economic and environmental indices. Energy Convers. Manag. 327, 119532. https://doi.org/10.1016/j.enconman.2025.119532.

Huang, Z., Yang, C., Zhou, X., et al., 2023. An improved TOPSIS-based multi-criteria decision-making approach for evaluating the working condition of the aluminum reduction cell. Eng. Appl. Artif. Intell. 117, 105599. https://doi.org/10.1016/j.engappai.2022.105599.

Hwang, C., Lai, Y., Liu, T., 1993. A new approach for multiple objective decision making. Comput. Oper. Res. 20, 889–899. https://doi.org/10.1016/0305-0548(93)90109-V.

Kalil, R.M., Santhoshkumar, S., Prathiba, R., et al., 2024. Internal combustion engine fuel synthesis, suitability, physical property evaluation using mixing models and backpropagation ANN algorithm. Eng. Appl. Artif. Intell. 132, 107970. https://doi.org/10.1016/j.engappai.2024.107970.

Kohavi, R., 1995. A study of cross-validation and bootstrap for accuracy estimation and model selection. In: International Joint Conference on Artificial Intelligence. https://dl.acm.org/doi/10.5555/1643031.1643047.

Kong, F., Liu, Z., Lin, C., et al., 2025. Experimental study and parameter optimization of desiccant wheel-assisted atmospheric water harvesting system based on NSGA-II. Energy Convers. Manag. 339, 119943.10.1016/j.enconman.2025.119943.

Lin, M., Chen, Z., Xu, Z., et al., 2021. Score function based on concentration degree for probabilistic linguistic term sets: an application to TOPSIS and VIKOR. Inf. Sci. 552, 270–290. https://doi.org/10.1016/j.ins.2020.10.061.

Lin, Y., Yeh, C., 2012. Multi-objective optimization for stochastic computer networks using NSGA-II and TOPSIS. Eur. J. Oper. Res. 218, 735–746. https://doi.org/10.1016/j.ejor.2011.11.028.

Liu, S., Agarwal, R., Sun, B., et al., 2021. Numerical simulation and optimization of injection rates and wells placement for carbon dioxide enhanced gas recovery using a genetic algorithm. J. Clean. Prod. 280, 124512. https://doi.org/10.1016/j.jclepro.2020.124512.

Lu, C., Zhang, M., Sun, Q., et al., 2025. Techno-economic assessment of surfactant Huff-n-Puff EOR in shale plays via multi-objective optimization. Geoenergy Sci. Eng. 244, 213449. https://doi.org/10.1016/j.geoen.2024.213449.

Mantel, N., 1967. The detection of disease clustering and a generalized regression approach. Cancer Res. 27, 209–220.

Manuel, V.M., Nelson, R.V., Eduardo, F., et al., 2023. Performance analysis of multi-objective simulated annealing based on decomposition. Math. Comput. Appl. 28, 38. https://doi.org/10.3390/mca28020038.

Morgan, A., Ampomah, W., Grigg, R., et al., 2023. Techno-economic life cycle assessment of CO_2-EOR operations towards net negative emissions at farnsworth field unit. Fuel 342, 127897. https://doi.org/10.1016/j.fuel.2023.127897.

Nguyen, Q.M., Onur, M., Alpak, F.O., 2024. Multi-objective optimization of subsurface CO_2 capture, utilization, and storage using sequential quadratic programming with stochastic gradients. Comput. Geosci. 28, 195–210. https://doi.org/10.1007/s10596-023-10213-6.

Rodriguez, P., Bautista, M.A., Gonzalez, J., et al., 2018. Beyond one-hot encoding: lower dimensional target embedding. Image Vis Comput. 75, 21–31. https://doi.org/10.1016/j.imavis.2018.04.004.

Shi, S., Xiong, H., 2024. Solving the multi-objective job shop scheduling problems with overtime consideration by an enhanced NSGA-II. Comput. Ind. Eng. 190, 110001. https://doi.org/10.1016/j.cie.2024.110001.

Sun, Y., Yen, G., Yi, Z., 2019. IGD indicator-based evolutionary algorithm for many-objective optimization problems. IEEE Trans. Evol. Comput. 23, 173–187. https://doi.org/10.1109/TEVC.2018.2791283.

Syed, F.I., Muther, T., Van, V.P., et al., 2022. Numerical trend analysis for factors affecting EOR performance and CO_2 storage in tight oil reservoirs. Fuel 316, 123370. https://doi.org/10.1016/j.fuel.2022.123370.

Vapnik, V., Golowich, S.E., Smola, A., 1996. Support vector method for function approximation, regression estimation and signal processing. In: NIPS'96: the 9th International Conference on Neural Information Processing Systems.

Wang, L., Li, Z., Adenutsi, C.D., et al., 2021. A novel multi-objective optimization method for well control parameters based on PSO-LSSVR proxy model and NSGA-II algorithm. J. Petrol. Sci. Eng. 196, 107694. https://doi.org/10.1016/j.petrol.2020.107694.

Wen, S., Wei, B., You, J., et al., 2023. Forecasting oil production in unconventional reservoirs using long short term memory network coupled support vector regression method: A case study. Petroleum 9, 647–657. https://doi.org/10.1016/j.petlm.2023.05.004.

Wen, S., Wei, B., You, J., et al., 2025. Rapid screening and optimization of CO_2 enhanced oil recovery operations in unconventional reservoirs: A case study. Petroleum 11, 188–200. https://doi.org/10.1016/j.petlm.2025.03.001.

Wu, K., Zhang, J., Feng, Q., et al., 2025. Co-optimization of well schedule and conformance control parameters assisted with Transformer-LSTM for CO_2-EOR and storage in oil reservoirs. Energy 331, 136891. https://doi.org/10.1016/j.energy.2025.136891.

Yue, P., Zhang, R., Sheng, J.J., et al., 2022. Study on the influential factors of CO_2 storage in low permeability reservoir. Energies 15, 344. https://doi.org/10.3390/en15010344.

Zhao, J., Wang, L., Wei, B., et al., 2025. CO_2 utilization and geological storage in unconventional reservoirs after fracturing. Engineering-PRC 48, 92–106. https://doi.org/10.1016/j.eng.2025.01.005.

Zhao, Z., Liu, B., Zhang, C., et al., 2019. An improved adaptive NSGA-II with multi-population algorithm. Appl. Intell. 49, 569–580. https://doi.org/10.1007/s10489-018-1263-6.

Zheng, W., Doerr, B., 2023. Runtime analysis for the NSGA-II: proving, quantifying, and explaining the inefficiency for many objectives. IEEE Trans. Evol. Comput. 28, 1442–1454. https://doi.org/10.1109/TEVC.2023.3320278.

Zhuang, X., Wang, W., Su, Y., et al., 2025. Life-cycle prediction and optimization of sequestration performance in CO_2 mixture huff-n-puff development for tight hydrocarbon reservoirs. Appl. Energy 388, 125618. https://doi.org/10.1016/j.apenergy.2025.125618.

Zhuang, X., Wang, W., Su, Y., et al., 2024. Multi-objective optimization of reservoir development strategy with hybrid artificial intelligence method. Expert Syst. Appl. 241, 122707. https://doi.org/10.1016/j.eswa.2023.122707.

Zuloaga, P., Yu, W., Miao, J., et al., 2017. Performance evaluation of CO_2 Huff-n-Puff and continuous CO_2 injection in tight oil reservoirs. Energy 134, 181–192. https://doi.org/10.1016/j.energy.2017.06.028.